Identification of Critical Hidden Failure Line Based on State-failure-network

Linzhi Li, Lu Liu, Hao Wu, Yonghua Song, Dunwen Song, and Yi Liu

***Abstract*—The hidden failures generally exist in power systems and could give rise to cascading failures. Identification of hidden failures is challenging due to very low occurrence probabilities. This paper proposes a state-failure-network (SF-network) method to overcome the difficulty. The SF-network is formed by searching the failures and states guided by risk estimation indices, in which only the failures and states contributing to the blackout risks are searched and duplicated searches are avoided. Therefore, sufficient hidden failures can be obtained with acceptable computations. Based on the state and failure value calculations in the SF-network, the hidden failure critical component indices can be obtained to quantify the criticalities of the lines. The proposed SF-network method is superior to common sampling based methods in risk estimation accuracy. Besides, the state and failure value calculations in the SF-network used to re-estimate the risks after deployment of measures against hidden failures need shorter time in comparison with other risk re-estimation methods. The IEEE 14-bus and 118-bus systems are used to validate the method.**

***Index Terms*—Blackout risk, cascading failure, hidden failure, state-failure-network method.**

I. Introduction

THE cascading failures in power systems can lead to large blackouts and cause severe losses to society [1], [2]. Among the past blackout events, more than 70% of major disturbances on power systems are caused by the hidden failures of protection systems [1], [3]. The hidden failure is a permanent defect that is undetectable during normal operation, but will cause a relay or a relay system to cut-off circuit elements incorrectly and inappropriately when exposed to a switching event [4]-[6]. To alleviate the impacts of hidden failures, in-time detection which activates emergency measures, and identification of critical elements, which helps improve the maintenance strategies and power grid planning, are the methods widely employed.

Some techniques have been proposed to detect the potential hidden failures before they occur. With the application of wide area measurement systems (WAMSs) and phasor measurement units (PMUs), the data analyses enable the operators to adopt on-line detection methods [7]-[9]. But the communication networks that transfer the data could also be subject to the hidden failures [10], [11]. In addition, measures need to be evaluated based on the economic costs and blackout risks, which are hard to be quantified by the on-line methods.

In order to minimize the potential costs and risks caused by hidden failures, the maintenance strategies are optimized to bolster the reliability of the protection systems [12], [13]. However, the line exposures of hidden failures [5], [14] and complex cascading failure propagations make it impracticable to estimate the impacts of hidden failures without cascading failure simulations.

As one of the factors that deteriorate the system during the cascading failures, the effects of hidden failures on system risks and reliability are studied in [5], [15]-[17]. Meanwhile, an increasing number of simulation models considering hidden failures are proposed in [18]-[21]. However, the literature does not distinguish between the critical hidden failure lines and the non-critical ones. To this end, the studies of hidden failures need certain numbers of samples, which is infeasible for normal sampling methods due to the low occurrence probabilities of hidden failures. Thus, the techniques such as importance sampling [3], [22] are introduced to focus on the events of interest and reduce the computation burden. Nevertheless, the sampling based methods estimate the risks by the expected losses of the samples, where the randomness of sampling can bring about inaccuracies in the estimated risks and the duplicated load flow calculations influence the efficiency. Therefore, an efficient method that can achieve more accurate risk estimation is needed.

In this paper, a state-failure-network (SF-network) method is proposed to identify the critical hidden failures and critical hidden failure lines. The SF-network method in this paper is improved based on the original proposed SF-network in [23], in order for the applicability in the study of hidden failures. Instead of using the simulated samples, the SF-network is formed by searching the failures and states, where the hidden failures of higher risks are singled out and duplicated searches are avoided. Once the SF-network is formed,

Manuscript received: February 5, 2020; revised: April 22, 2020; accepted: July 23, 2020. Date of CrossCheck: July 23, 2020. Date of online publication: January 25, 2021.

This work was partly supported by the State Grid Corporation of China (No. SGTYHT/17-JS-199XT71-18-019).

L. Li, L. Liu, H. Wu (corresponding author), and Y. Song are with the College of Electrical Engineering, Zhejiang University, Hangzhou, China, and Y. Song is also with the Department of Electrical and Computer Engineering, University of Macau, Macau, China (e-mail: lilinzhilee@zju.edu.cn; liuluzjuee@zju.edu.cn; zjuwuhao@zju.edu.cn; yhsongcn@zju.edu.cn).

D. Song is with China Electric Power Research Institute, Beijing, China (e-mail: songdw@epri.sgcc.com.cn).

Y. Liu is with State Grid Henan Electric Power Company, Zhengzhou, China (e-mail: liuyi1@ha.sgcc.com.cn).

DOI: 10.35833/MPCE.2020.000056

the hidden failure critical component indices (hCCIs) that quantify the critical extents of the lines can be obtained. Therefore, the critical hidden failure lines are identified among the ones with high hCCI. The value calculations in the SF-network also offer an efficient way to re-estimate the risks and verify the identification consequences.

The rest of the paper is organized as follows. Section II illustrates the model of hidden failure and the cascading failure simulation considering hidden failures. Then the SF-network method is introduced in Section III. Finally, two cases are used to validate the proposed method in Section IV.

II. Cascading Failure Simulation Considering Hidden Failures

A. Model of Hidden Failures

The undetected defects of the relays can give rise to the hidden failures. If any adjacent line of line l (connected to the same bus as line l) fails, the defective relay of line l will be exposed and line l may be falsely tripped [5]. In fact, an exposure is the state when a line becomes probable to fail due to the failure of its adjacent lines, in which a nearby failure can cause the mal-operation of the defective relay when the relay reacts to the fault transient [24]. Once exposed, the lines are subject to hidden failures. As the probability of a single hidden failure is small (lower than 10^{-2}), the multiple hidden failures with much smaller probabilities are not considered in this paper. That is, only single hidden failures are taken into account in the model.

During a cascading event, line exposure can occur multiple times to a single line. However, the hidden failures of the lines are more likely to occur on the first exposure than on the subsequent exposures [5]. For simplify, we follow the line exposure in [5] that hidden failure can occur only at the first line exposure with hidden failure probability p^h. More specifically, let p_l^{H} be the hidden failure probability of line l, $\mathcal{S}_l^{\mathrm{AL}}$ denotes the set of adjacent lines of line l, and t_l^{E} denote the exposure count which is the times that a line is exposed during a cascading event. Then, after line k fails, we can have:

$$p_l^{\mathrm{H}} = \begin{cases} p^h & k \in \mathcal{S}_l^{\mathrm{AL}} \text{ and } t_l^{\mathrm{E}} = 1 \\ 0 & \text{otherwise} \end{cases} \tag{1}$$

B. Cascading Failure Simulation Method Considering Hidden Failures

The cascading failures considering hidden failures are simulated by a DC power flow based simulator modified from the simulator in [24], [25]. The procedure of the simulation, which is shown in Fig. 1, can be illustrated as follows.

Step 1: input the initial operation point of the power system.

Step 2: set initial contingencies to trigger the cascading failures.

Step 3: detect islands. If new islands are detected, re-balance the generation and loads in each island. Otherwise, re-dispatch the islands based on the dispatch method in [26] to eliminate line overloads.

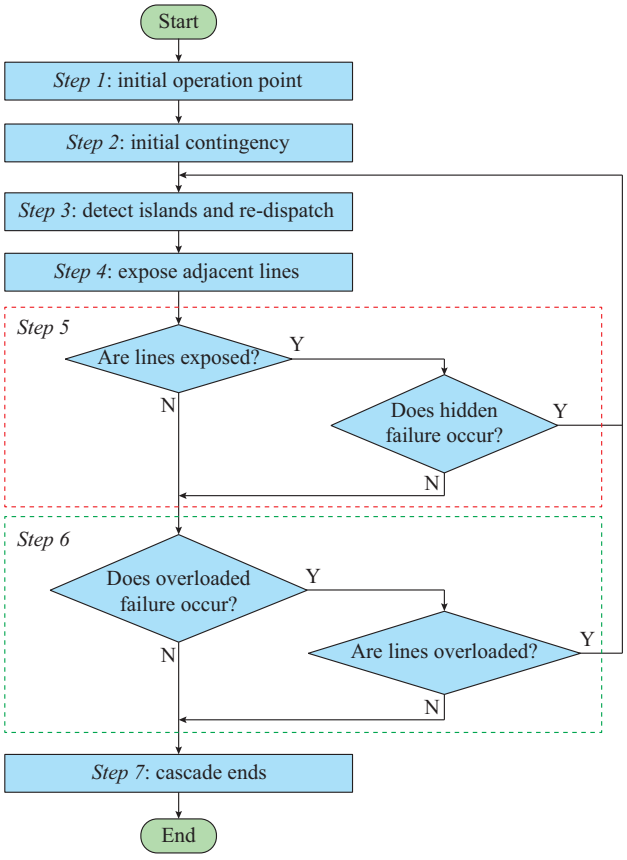

Fig. 1. Flow chart of cascading failure simulation considering hidden failures.

Step 4: expose the adjacent lines of the failed lines.

Step 5: check the exposed lines according to *Step 1*. If no line is exposed, go to *Step 6*. For the exposed lines whose $p^{\mathrm{H}} > 0$, select a line to trip as the hidden failure based on the Roulette-Wheel algorithm [27], [28]. Specifically, the simulated probability of the hidden failure of an exposed line l is:

$$p_l^{\mathrm{HW}} = (1 - p_0^{\mathrm{HW}}) \frac{p_l^{\mathrm{H}}}{\sum_{l=1}^{n_1} p_l^{\mathrm{H}}} \tag{2}$$

$$p_0^{\mathrm{HW}} = \prod_{l=1}^{n_1} (1 - p_l^{\mathrm{H}}) \tag{3}$$

where n_1 is the number of lines in the system; and p_0^{HW} is the simulated probability of no hidden failure.

According to *Steps 2* and *3*, it always holds that $p_0^{\mathrm{HW}} + \sum_{l=1}^{n_1} p_l^{\mathrm{HW}} = 1$. If any hidden failure occurs, go to *Step 3*. Otherwise, go to *Step 6*.

Step 6: check the overloaded lines. In fact, the lines whose loads are close to their capacities are taken as overloaded and can fail in a certain probability [5], [18]. Similarly, according to the Roulette-Wheel algorithm, the simulated probability of an overloaded failure p_l^{FW} is:

$$p_l^{\mathrm{FW}} = (1 - p_0^{\mathrm{FW}}) \frac{p_l^{\mathrm{F}}}{\sum_{l=1}^{n_1} p_l^{\mathrm{F}}} \tag{4}$$

$$p_0^{\mathrm{FW}} = \prod_{l=1}^{n_l}(1-p_l^{\mathrm{F}}) \tag{5}$$

where p_l^{F} is a load dependent variable whose value is between 0 and 1 when the line is overloaded, and equals to 0 otherwise [18], [29]; and p_0^{FW} is the simulated probability of no overloaded failure.

According to *Steps 4* and *5*, it always holds that $p_0^{\mathrm{FW}} + \sum_{l=1}^{n_l} p_l^{\mathrm{FW}} = 1$. When any line is tripped, go to *Step 3*. If no line is overloaded or tripped, go to *Step 7*.

Step 7: the cascade ends, and the total loss of the chain z is recorded.

The simulation offers a cascading failure sample after the cascade ends.

It is worth noting that the events of hidden failures show higher priority than those of overloaded failures in the simulation procedure. In other words, the overloaded failure can only occur when no hidden failure occurs at the current stage.

C. Major Defects of Sampling Based Methods

In general, the risk estimation needs enormous Monte-Carlo (MC) samples to obtain the expected losses as:

$$r = \frac{1}{N_{\mathrm{M}}}\sum_{i=1}^{N_{\mathrm{M}}} z_i \tag{6}$$

where N_{M} is the number of samples; z_i is the loss of the i^{th} simulation sample; and r is the risk of the power system. Reference [5] argues that hidden failures can weaken the system and increase the blackout risk. Figure 2 shows the risk of the IEEE 14-bus system estimated by the simulations with and without hidden failures. The blackout risk without hidden failures is 24.077 MW, whereas the risk rises to 24.338 MW when hidden failures ($p^{\mathrm{h}} = 0.01$) are considered. Although the rise of risk looks mild, the influence of hidden failures can be better reflected by the complementary cumulative distribution function (CCDF) of the blackouts as shown in Fig. 3. It is shown that the hidden failures mainly give rise to the risk of the severe blackouts whose losses exceed 30% of the total loads, and cause the losses of blackouts over 53.93%. Therefore, the total increase of risk caused by the hidden failures seems low, but it is of great significance to cope with the hidden failures for reducing the occurrences of large-scale blackouts.

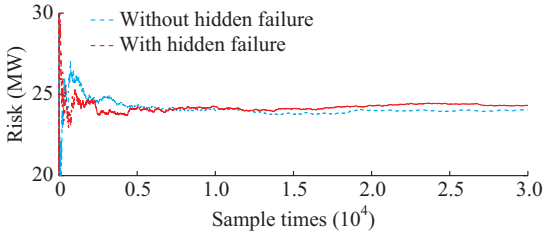

Fig. 2. Risks estimated by cascading failure models with and without hidden failures.

However, sampling based methods such as the MC have two major defects. One is that collecting sufficient samples of hidden failures to identify the critical hidden failures can be infeasible due to the very low occurrence probabilities.

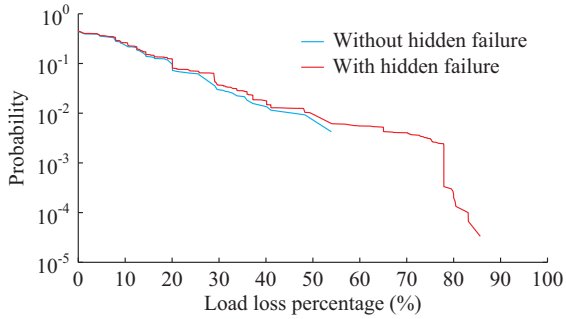

Fig. 3. CCDFs of blackouts estimated by simulations with and without hidden failures.

Figure 4 shows the mean values of the hidden failures, failures and exposed lines among the simulated samples. The comparison between the hidden failures and exposed lines is sharp, which manifests that only very few exposed hidden failures are sampled in the MC sampling method.

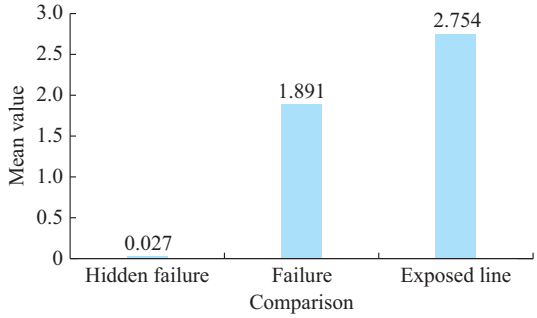

Fig. 4. Mean values of recorded failures and exposed line among samples of IEEE 14-bus system.

Besides, it should also be noted that the difference between the estimated risks of scenarios in Fig. 2 is not very high. Accordingly, for a scenario where the hidden failure probability of any line changes, the corresponding risk change might not be accurately estimated due to the sampling randomness before the convergence.

Therefore, a method is needed to collect sufficient hidden failures and more accurately estimate the blackout risks, and the SF-network method proposed by the authors in their previous work [24] can be improved to meet these requirements.

III. SF-NETWORK METHOD

A. States and Failures in SF-network

The structure of SF-network is mainly formed by the states and failures, which can be obtained by the cascading failure chains [24].

First, a k-length cascading failure chain comprised of the failure sequence $\{f_{(1)}, f_{(2)}, \ldots, f_{(k)}\}$ and final loss is denoted by $f_{(1)} \rightarrow f_{(2)} \rightarrow \ldots \rightarrow f_{(k)} \rightarrow z$, where the subscripts in brackets are the occurrence order of the failures. Then the states are denoted as vectors $\boldsymbol{s}_0, \boldsymbol{s}_1, \ldots, \boldsymbol{s}_k$, and the k^{th} state of the failure chain is defined as $\boldsymbol{s}_k = [f_{(1)}, f_{(2)}, \ldots, f_{(k)}]$.

In addition, we denote the initial state where no failure occurs as $\boldsymbol{s}_0$, and the ending mark of a failure chain as $f_{(0)}$. Then, recombine the states and corresponding failures as a

tuple sequence: $(\boldsymbol{s}_0,f_{(1)}),(\boldsymbol{s}_1,f_{(2)}),\ldots,(\boldsymbol{s}_{k-1},f_{(k)}),(\boldsymbol{s}_k,f_{(0)})$.

The subscripts of the state vectors are the stage numbers, which are also the numbers of failed lines.

Secondly, nodes and edges are used to signify the states and failures, respectively. The nodes and edges are joined based on the tuple sequences as shown in Fig. 5.

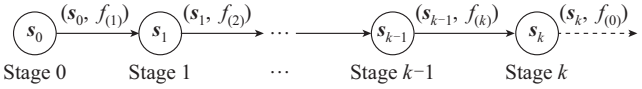

Fig. 5. State-failure sequence.

We can get the structure of the SF-network from tuple sequences as illustrated in Fig. 6, where $\boldsymbol{s}_{k(j)}$ is the j^{th} state at the k^{th} stage.

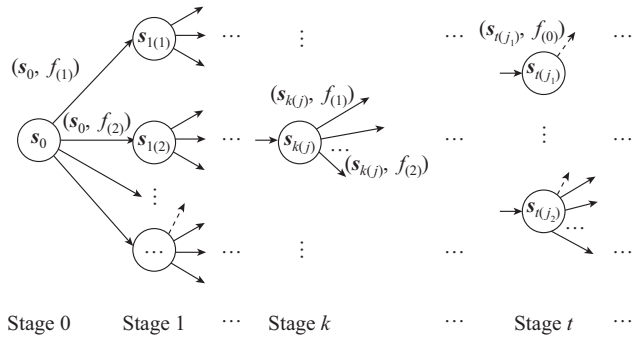

Fig. 6. Structure of SF-network.

As in the figure, the SF-network originates at the initial state $\boldsymbol{s}_0$, spreads along the subsequent chains of states and failures, and terminates at the states with $f_{(0)}$.

The states in this paper differ from those in the original SF-network in [24], so as to reflect the failure sequences.

B. Risk Estimation in SF-network

In the authors' previous work [17], forming the SF-network needs numerous cascading failure chains produced by cascading failure simulations. However, the method based on sampled failure chains cannot well cope with the hidden failures as discussed in Section II-C, so the way to form the SF-network needs to be changed.

In the improved SF-network, the impact of sampling randomness on the risk estimation is eliminated. The loss of the i^{th} failure chain z_i in (6) is the sum of the losses that occur at the states along the failure chain and can be formulated as:

$$\begin{cases} z_i=\breve{z}(\boldsymbol{s}_1^i)+\breve{z}(\boldsymbol{s}_2^i)+\ldots+\breve{z}(\boldsymbol{s}_k^i) \\ \boldsymbol{s}_k^i=[f_{(1)}^i \quad f_{(2)}^i \quad \cdots \quad f_{(k)}^i] \end{cases} \tag{7}$$

where $\breve{z}(\boldsymbol{s}_k^i)$ is the loss that occurs at state $\boldsymbol{s}_k^i$.

Substituting (7) into (6), we can get:

$$r=\frac{1}{N_{\text{M}}}\sum_{i=1}^{N_{\text{M}}}(\breve{z}(\boldsymbol{s}_1^i)+\breve{z}(\boldsymbol{s}_2^i)+\ldots+\breve{z}(\boldsymbol{s}_k^i)) \tag{8}$$

Since the similar states in the failure chains, which share similar failure sequences, are merged into a single state in the SF-network, denoting the number of the gathered state $\boldsymbol{s}_{k(j)}$ as $N_{\boldsymbol{s}_{k(j)}}$. Thus, (8) can be rewritten as:

$$r=\frac{1}{N_{\text{M}}}(N_{\boldsymbol{s}_{1(1)}}\breve{z}(\boldsymbol{s}_{1(1)})+N_{\boldsymbol{s}_{1(2)}}\breve{z}(\boldsymbol{s}_{1(2)})+\ldots+N_{\boldsymbol{s}_{k_m(j)}}\breve{z}(\boldsymbol{s}_{k_m(j)}))=$$
$$\sum_{j=1}^{N_1^s}\frac{N_{\boldsymbol{s}_{1(j)}}}{N_{\text{M}}}\breve{z}(\boldsymbol{s}_{1(j)})+\sum_{j=1}^{N_2^s}\frac{N_{\boldsymbol{s}_{2(j)}}}{N_{\text{M}}}\breve{z}(\boldsymbol{s}_{2(j)})+\ldots+\sum_{j=1}^{N_{k_m}^s}\frac{N_{\boldsymbol{s}_{k(j)}}}{N_{\text{M}}}\breve{z}(\boldsymbol{s}_{k_m(j)}) \tag{9}$$

where k_m is the final stage of SF-network; and $N_{k_m}^s$ is the number of states at the k_m^{th} stage.

As the number of samples N_{M} increases, the fraction $N_{\boldsymbol{s}_{k(j)}}/N_{\text{M}}$ will converge to the corresponding occurrence probability of $\boldsymbol{s}_{k(j)}$, $\Pr(\boldsymbol{s}_{k(j)})$. Thus, we have:

$$\lim_{N_{\text{M}}\to\infty}\frac{N_{\boldsymbol{s}_{k(j)}}}{N_{\text{M}}}=\Pr(\boldsymbol{s}_{k(j)}) \tag{10}$$

$\Pr(\boldsymbol{s}_{k(j)})$ can be derived from:

$$\Pr(\boldsymbol{s}_{k(j)})=\Pr(f_{(1)})\Pr(f_{(2)}|f_{(1)})\ldots\Pr(f_{(k)}|f_{(1)}\ldots f_{(k-1)}) \tag{11}$$

Therefore, the accurate estimated risk can be obtained by the sum of the risks of the states in the SF-network, which is more accurate than the estimated risk of random samples derived from (6).

$$r=\sum_{j=1}^{N_1^s}\Pr(\boldsymbol{s}_{1(j)})\breve{z}(\boldsymbol{s}_{1(j)})+\sum_{j=1}^{N_2^s}\Pr(\boldsymbol{s}_{2(j)})\breve{z}(\boldsymbol{s}_{2(j)})+\ldots+$$
$$\sum_{j=1}^{N_{k_m}^s}\Pr(\boldsymbol{s}_{k_m(j)})\breve{z}(\boldsymbol{s}_{k_m(j)}) \tag{12}$$

C. Form SF-network by Searching

According to (12), the risk can be obtained by searching the states of the SF-network and summing the risks of the states. Instead of sampling the cascading failure chains randomly based on their probabilities, the failures of high risks and the hidden failures leading to high losses are the interest of this paper. Thus, we introduce the risk estimation indices to guide the searching process.

When the search reaches a state, the risk estimation indices indicate the risks of the failures of the operating lines at the state. To calculate the risk estimation indices, the failure probabilities of the lines and estimated losses are worked out as follows.

1) Failure probability calculation: according to Section II-B, the occurrence of hidden failures shows higher priority than that of the overloaded failures at a new stage. However, all the failures can be taken as mutually exclusive independent events, so the failure probability of line l at state $\boldsymbol{s}_{k(j)}$ can be obtained by:

$$\Pr(\boldsymbol{s}_{k(j)},f_l)=\Pr^{\text{H}}(\boldsymbol{s}_{k(j)},f_l)+\Pr^{\text{F}}(\boldsymbol{s}_{k(j)},f_l) \tag{13}$$

$$\begin{cases} \Pr^{\text{H}}(\boldsymbol{s}_{k(j)},f_l)=p_l^{\text{HW}} \\ \Pr^{\text{F}}(\boldsymbol{s}_{k(j)},f_l)=p_0^{\text{HW}}p_l^{\text{FW}} \end{cases} \tag{14}$$

where $\Pr^{\text{H}}(\boldsymbol{s}_{k(j)},f_l)$ is the hidden failure probability of line l at state $\boldsymbol{s}_{k(j)}$; $\Pr^{\text{F}}(\boldsymbol{s}_{k(j)},f_l)$ is the overloaded failure probability of line l at state $\boldsymbol{s}_{k(j)}$; and f_l is the failure of line l.

Particularly, the probability of no failure can be derived from (3) and (5) as:

$$\Pr(\boldsymbol{s}_{k(j)},f_{(0)})=p_0^{\text{HW}}p_0^{\text{FW}} \tag{15}$$

Once line l is selected and fails, the probability of the next state $\boldsymbol{s}_{k+1(j')}$ after line l fails is obtained by:

$$\Pr(\boldsymbol{s}_{k+1(j')})=\Pr(\boldsymbol{s}_{k(j)})\Pr(\boldsymbol{s}_{k(j)},f_l) \tag{16}$$

2) Estimated loss calculation: the failures can cause losses. In this paper, the loss of system splitting σ^{α} and loss of overloading σ^{β} are considered. At state $\boldsymbol{s}_{k(j)}$, both σ^{α} and σ^{β} can be calculated based on the admittance matrix of the system Y and the Penrose-Moore pseudo-inverse of Y as introduced in [30], [31]. If the failure of the line causes the system splitting, it means the line is cut off, and its σ^{α} can be obtained and its $\sigma^{\beta}=0$. Otherwise, its σ^{β} should be calculated and its $\sigma^{\alpha}=0$. Thus, for an arbitrary line l at $\boldsymbol{s}_{k(j)}$, its estimated loss is:

$$\sigma(\boldsymbol{s}_{k(j)},f_l)=\alpha\sigma^{\alpha}(\boldsymbol{s}_{k(j)},f_l)+\beta\sigma^{\beta}(\boldsymbol{s}_{k(j)},f_l) \tag{17}$$

where α is the system splitting loss coefficient; and β is the overloading loss coefficient. The values of α and β depend on the loss preference of the operator, and their sum is 1. If the loss of system splitting requires more attention, they should be set as $\alpha>\beta$, and vice versa. Without loss of generality, the two kinds of estimated losses are treated equally by setting $\alpha=\beta=0.5$ in this paper.

Given the failure probability and estimated loss, the risk estimation index of line l can be obtained by:

$$\rho(\boldsymbol{s}_{k(j)},f_l)=\Pr(\boldsymbol{s}_{k(j)},f_l)\sigma(\boldsymbol{s}_{k(j)},f_l) \tag{18}$$

Hence, the searching is guided to the failures with higher risk estimation indices so that the states of high risks can be added into (12). Specifically, the failures at a certain state are searched based on the probabilities derived from the Roulette-Wheel algorithm and the risk estimation indices obtained by (18). Thus, the failures with higher indices are more probable to be searched. When there are no overloads/exposures or the probability of the searched failure chain is below a threshold $\Pr_{\min}$, the search on the current failure chain terminates and the search continues on a new failure chain. The search avoids duplicated failure chains by updating the risk estimation indices after finishing searching a failure chain [31], which saves the computation time. At a new state, the state as well as the operation information is recorded in the SF-network. Thus, in the following searches, the redispatch and risk estimation calculations can be avoided by retrieving the state directly from the SF-network, which further curtails the computation burdens. Figure 7 shows the searching procedure forming the SF-network.

D. State and Failure Value Calculations in SF-network

After forming the SF-network, the state values (abbreviated as S-value) and failure values (abbreviated as F-value) can be worked out by the SF-network value calculations [24]. Specifically, the S-value and F-value are calculated as follows.

1) S-value calculation:

$$S(\boldsymbol{s}_{k(j)})=\sum_{f_l\in\Gamma^{\mathrm{f}}_{k(j)}}\Pr(\boldsymbol{s}_{k(j)},f_l)F(\boldsymbol{s}_{k(j)},f_l) \tag{19}$$

where $\Gamma^{\mathrm{f}}_{k(j)}$ is the set of failures that occur at $\boldsymbol{s}_{k(j)}$; and $F(\boldsymbol{s}_{k(j)},f_l)$ is the F-value of the failure f_l at $\boldsymbol{s}_{k(j)}$.

2) F-value calculation: the F-value of the failure f_l equals to the S-value of its next state, which is denoted as $\boldsymbol{s}_{k+1(\cdot)}$. The F-value of $f_{(0)}$ equals to the total loss of the system at $\boldsymbol{s}_{k(j)}$.

$$F(\boldsymbol{s}_{k(j)},f_l)=\begin{cases}z(\boldsymbol{s}_{k(j)}) & l=0\\ S(\boldsymbol{s}_{k+1(\cdot)}) & l\neq 0\end{cases} \tag{20}$$

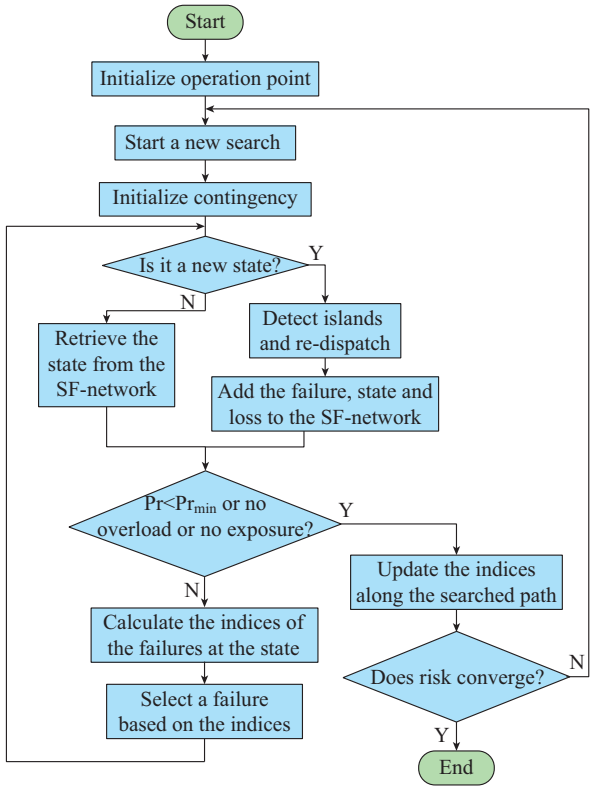

Fig. 7. Searching procedure of SF-network.

where $z(\boldsymbol{s}_{k(j)})$ is the loss of state $\boldsymbol{s}_{k(j)}$.

The calculation starts at the states where cascades terminate, and performs successively from larger stages to smaller ones (from right to left in Fig. 6). The algorithm can be briefly illustrated as follows:

1) Get the F-value of $f_{(0)}$ at the backmost state at the maximal stage in the SF-network according to (20). Then, the S-value of the backmost state equals to the F-value of the $f_{(0)}$ according to (19).

2) Move forward to the next stage. According to (20), the F-values of the failures all equal to the S-values of their next states, which have been obtained at the previous stage. Then, the S-values of the states at the current stage are worked out based on (19).

3) Continue the calculation until the first stage. Then $S(\boldsymbol{s}_0)$, the S-value of initial state $\boldsymbol{s}_0$, is finally worked out and equals to the system blackout risk.

After state and failure value calculations of the SF-network, every state and failure gets a value that quantifies the expected loss after its occurrence.

E. Identify Critical Hidden Failures in SF-network

The critical failures at a state can be identified as the ones whose F-values are higher than the S-value of the state. The critical component index (CCI) can be calculated by summing up the risks of the critical failures in the SF-network.

$$R_l=\sum_{k=k_0}^{\infty}\sum_{j=1}^{N_k}\sum_{f_l\in\Gamma^{\mathrm{f}}_{k(j)}}I(\boldsymbol{s}_{k(j)},f_l)\Pr(\boldsymbol{s}_{k(j)},f_l)F(\boldsymbol{s}_{k(j)},f_l) \tag{21}$$

$$I(\boldsymbol{s}_{k(j)},f_l)=\begin{cases}1 & F(\boldsymbol{s}_{k(j)},f_l)>S(\boldsymbol{s}_{k(j)})\\ 0 & F(\boldsymbol{s}_{k(j)},f_l)\le S(\boldsymbol{s}_{k(j)})\end{cases} \tag{22}$$

where $I(\boldsymbol{s}_{k(j)},f_l)$ is the indicator function; N_k is the number of states at the k^{th} stage; and k_0 is the first stage after the initial outages.

Since the probabilities of hidden failures and overloaded failures are distinguishable in the SF-network, the hCCI similar to the CCI can be obtained by:

$$R_l^{\text{H}} = \sum_{k=k_0}^{\infty}\sum_{j=1}^{N_k}\sum_{f_l\in\Gamma_{k(j)}^{\text{f}}} I(\boldsymbol{s}_{k(j)},f_l)\Pr^{\text{H}}(\boldsymbol{s}_{k(j)},f_l)F(\boldsymbol{s}_{k(j)},f_l) \tag{23}$$

Thus, the lines with high R_l^{H} are the critical hidden failure lines.

F. Risk Re-estimation after Probability Changes in SF-network

Once the critical hidden failure lines are identified, the result should be verified to validate the SF-network method. To this end, the risk of the system after the critical lines are upgraded needs to be re-estimated to quantify the effect. Since the risk assessment can measure the robustness of the power system to withstand the hidden failures and cascading failures, upgrading the most critical lines should be the most effective in increasing the robustness and decreasing the risks [1], [24]. The measures to upgrade lines in the real system can include relay parameter corrections and maintenances, which decrease the hidden failure occurrence probabilities. Therefore, the verification demands another run of the searching procedure for the new SF-network with decreased hidden failure probabilities.

However, the sufficiently searched SF-network has already had the information of states and cascading failures. Thus, the new risks can be re-calculated by the state and failure value calculations in the SF-network with changed failure probabilities. More specifically, the hidden failure probability of line l is decreased from p_l^{H} to p'^{H}_l, then the probabilities of the failures in SF-network are all re-calculated according to (2)(4), (13), (14). Afterwards, the calculation algorithm in Section III-D obtains a new S-value of $\boldsymbol{s}_0$, which is the new risk r'. The risk drop between the original risk r and the new risk r' is derived from

$$\Delta r = r - r' \tag{24}$$

where upgrading the most critical hidden failure is expected to achieve the largest Δr.

Compared with the repetitive load flow and re-dispatch computations during the search to form the new SF-network, the re-calculations in the SF-network are all algebraic calculations which only take very short time. Besides, the efficiency of risk re-estimation also makes the SF-network method superior to the MC sampling methods.

G. Impact of Hidden Failure Probability Changes

As hidden failure probability changes only impact the probabilities in the SF-network, (24) can be rewritten as:

$$\Delta r = r - r' = \sum_{j=1}^{N_1^s}(\Pr(\boldsymbol{s}_{1(j)}) - \Pr'(\boldsymbol{s}_{1(j)}))\check{z}(\boldsymbol{s}_{1(j)}) + \ldots + \sum_{j=1}^{N_{k_m}^s}(\Pr(\boldsymbol{s}_{k_m(j)}) - \Pr'(\boldsymbol{s}_{k_m(j)}))\check{z}(\boldsymbol{s}_{k_m(j)}) \tag{25}$$

where k_m is the final stage of SF-network. It indicates that the system risk changes can be summed up by the risk changes of the states. Though the Δr is expected to be positive when the failure probabilities of critical lines are decreased, some of the items in (25) can be negative, indicating the risks increase of some states.

The reason lies in the interaction effects of the probabilities of the line failures at a state. Since it always holds at an arbitrary state $\boldsymbol{s}$ that:

$$\sum_{f_l\in\Gamma^{\text{f}}}\Pr(\boldsymbol{s},f_l) = 1 \tag{26}$$

where Γ^{f} is the set of failures that occur at state $\boldsymbol{s}$.

Thus, the probability decreases of some failures might increase the occurrence probabilities of the other failures. According to the probability relationship between the failures and states in (16), the Pr' items can be either larger or smaller than the corresponding Pr items in (25). Then, (25) can be rewritten as:

$$\Delta r = (\ldots + (\Pr^{+}(\boldsymbol{s}_{k(j)}) - \Pr'^{+}(\boldsymbol{s}_{k(j)}))\check{z}(\boldsymbol{s}_{k(j)}) + \ldots) + (\ldots + (\Pr^{-}(\boldsymbol{s}_{n(m)}) - \Pr'^{-}(\boldsymbol{s}_{n(m)}))\check{z}(\boldsymbol{s}_{n(m)}) + \ldots) = \Delta r^{+} + \Delta r^{-} \tag{27}$$

where $\boldsymbol{s}_{n(m)}$ is the m^{th} state in the n^{th} state in SF-network; $\Pr^{+}(\boldsymbol{s}_{k(j)})$ and $\Pr'^{+}(\boldsymbol{s}_{k(j)})$ are the failure probabilities of state $\boldsymbol{s}_{k(j)}$ with the risk $\Delta r^{+} > 0$ before and after SF-network updating, respectively; $\Pr^{-}(\boldsymbol{s}_{n(m)})$ and $\Pr'^{-}(\boldsymbol{s}_{n(m)})$ are the failure probabilities of state $\boldsymbol{s}_{n(m)}$ before and after SF-network updating, respectively; Δr^{+} and Δr^{-} are the risk values greater and less than 0, respectively. Therefore, if $|\Delta r^{-}| > |\Delta r^{+}|$, Δr will be negative and the system risk will increase after the hidden failure probabilities are decreased. In general, the negative Δr is more likely to result from decreasing the probabilities of non-critical hidden failure lines, which increases the probabilities of critical failures at the corresponding states.

IV. Case Study

The test program is developed and tested in MATLAB on a computer with 2.4 GHz processor and 32 GB RAM. In both the cases below, $p^{\text{h}} = 0.01$ and $p_l^{\text{F}} = 0.7$ for all lines, and $\Pr_{\min} = 10^{-8}$. The system data are accessible in [32].

A. Case 1: IEEE 14-bus System

The initial operation point is set based on the settings in [33], where the loads are scaled up to 150% of their original values. The initial contingencies are random $N-1$ contingencies.

It takes 3546 searches and 170.17 s to form the SF-network, and the estimated risk is 26.63 MW. The risks estimated by four groups of random MC samples (each group takes about 680 s) and the SF-network are given in Fig. 8. The MC sampling risks gradually converge to the risk obtained by the SF-network, but the estimated risks vary from 24.15 MW to 24.96 MW, where the maximal fluctuation of 0.81 MW is larger than the risk variation caused by hidden failures shown in Fig. 2. Therefore, the risk fluctuations of MC sampling method can cover the risk changes caused by hidden failure probability adjustments, which hinders the accurate verification of the identified critical hidden failure lines.

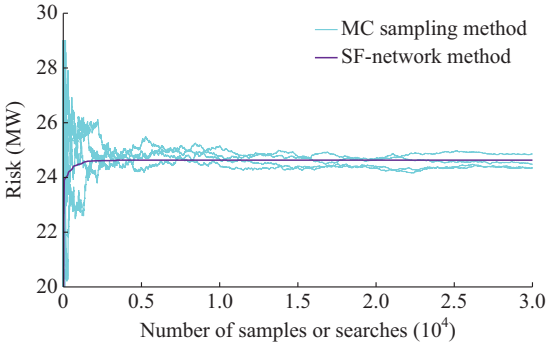

Fig. 8. Cascading failure risks estimated by MC sampling method and SF-network method in IEEE 14-bus system.

After the state and failure value calculations in the SF-network, the CCIs are calculated according to (21) and listed in Table I, where the CCIs of the lines derived from the SF-network without considering hidden failures are also given for comparison. The rankings of the lines with and without the hidden failures considered are almost the same. However, the hidden failures can considerably raise the complexity of the cascading failures. The lines with zero CCIs in the right columns do not fail when hidden failures are not considered, whereas they all become risky when hidden failures are considered.

TABLE I
CCIs of Lines In IEEE 14-bus System

With hidden failures			Without hidden failures		
Ranking	Line	CCI	Ranking	Line	CCI
1	7	12.9913	1	3	12.8719
2	3	12.9658	2	7	11.7990
3	4	10.7422	3	4	10.8183
4	8	5.7305	4	8	5.6913
5	10	5.0721	5	10	4.2686
6	1	4.0909	6	14	3.6455
7	14	3.7373	7	9	2.9149
8	9	2.9575	8	1	2.8073
9	6	2.0169	9	6	1.9545
10	13	1.6154	10	13	1.5435
11	12	1.3112	11	12	1.3093
12	5	0.7419	12	5	0.7231
13	2	0.4933	13	2	0.3599
14	20	0.0602	14	11	0
15	18	0.0432	14	15	0
16	11	0.0424	14	16	0
17	16	0.0168	14	17	0
18	15	0.0067	14	18	0
19	17	0.0061	14	19	0
20	19	0.0006	14	20	0

The hCCIs are obtained according to (23) and listed in Table II. In the table, line 5 is remarkable for its top ranking compared with the low ranking in Table I. We draw the top ranking 5 lines of both tables with high CCIs and hCCIs in green and red in Fig. 9, respectively. It can be seen that some of the identified critical lines have both high CCIs and hCCIs, which indicates that the critical overloaded failure lines can also be critical when they are exposed. Besides, the identified critical lines center around the generator buses. However, for the critical hidden failure lines which are not the critical overloaded failure lines, like line 5, they are critical because the failures of their adjacent lines are critical and their failures following up can notably deteriorate the system.

TABLE II
hCCIs of Lines in IEEE 14-bus System

Ranking	Line	hCCI	Ranking	Line	hCCI
1	4	0.355172	11	13	0.055659
2	5	0.266609	12	2	0.054695
3	3	0.160620	13	14	0.032550
4	8	0.130359	14	17	0.021565
5	9	0.113619	15	19	0.019921
6	10	0.109482	16	12	0.019627
7	11	0.100151	17	16	0.017825
8	7	0.091987	18	1	0.016431
9	6	0.075246	19	20	0.001338
10	15	0.063552	20	18	0.000292

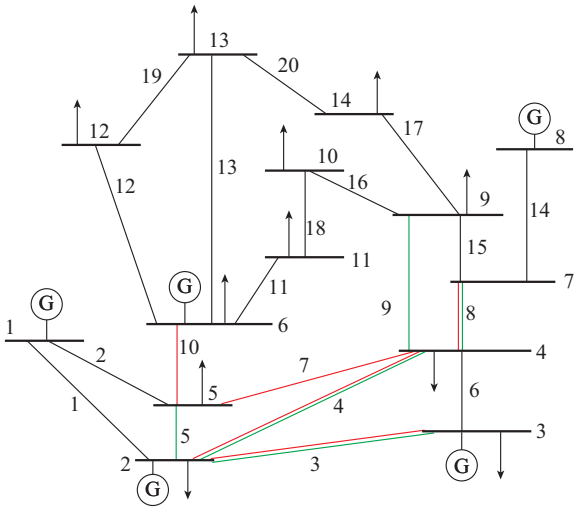

Fig. 9. Identified critical lines in IEEE 14-bus system.

To verify the identified critical hidden failure lines, three groups of lines are chosen to be upgraded in different scenarios according to their rankings in Table II, where their hidden failure probabilities are decreased from 0.01 to 0.001. Lines 4, 5, 3 are the top-ranking lines; lines 6, 15, 13 are the middle-ranking lines; and lines 1, 20, 18 are the low-ranking lines. Their risk drops are given in Table III, which show that upgrading the most critical hidden failure lines (the top-ranking lines) can reduce most of risks.

The complementary cumulative distribution functions (CCDFs) of the blackouts in the scenarios are given in Fig. 10, where the main parts of the CCDFs of are very close. However, the tails of the CCDFs which correspond to the probabilities of the severe blackouts shows notable differences. We take the blackouts with losses larger than 300 MW as

the severe blackouts. Then, the occurrence numbers of the severe blackouts are 23, 18, 12 and 4 in the original, low-ranking, middle-ranking and top-ranking scenarios, respectively. According to [34], given that the occurrence number of the severe blackouts in the top ranking scenario is 4, if the occurrence numbers of the severe blackouts in the other scenarios are larger than 10, it can be concluded that the occurrence probabilities of the severe blackouts in the other scenarios are higher than that in the top-ranking scenario with a confidence level of 95%. Therefore, we can conclude that the occurrence probability of the severe blackouts in the top-ranking scenario is the lowest among the four scenarios with a confidence level of 95%, and upgrading the identified most critical lines can achieve the highest probability decreases of blackouts.

TABLE III
RISK VARIATION DUE TO HIDDEN FAILURE PROBABILITY CHANGES OF IEEE 14-BUS SYSTEM

Line group	Lines	Δr	Δr^+	Δr^-
Top-ranking	4, 5, 3	0.2548	0.3860	–0.1312
Middle-ranking	6, 15, 13	0.0066	0.1054	–0.0989
Low-ranking	1, 20, 18	–0.0310	0.0219	–0.0529

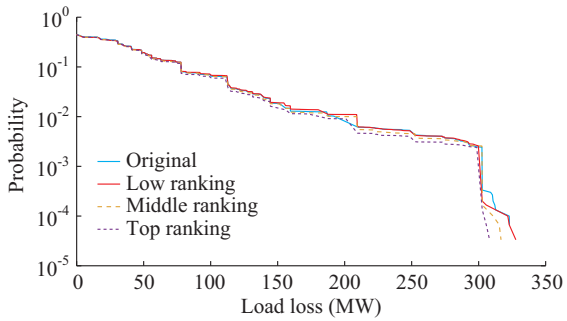

Fig. 10. CCDFs of blackouts after upgrading different groups of lines in IEEE 14-bus system.

It can be also seen that the hidden failures have greater influence on the probabilities of blackouts with larger scale than those of blackouts with smaller scale.

Here, each risk re-estimation by the calculations in the SF-network takes only about 2 s, which demonstrates the efficiency of the SF-network method. The upgrading of the top-ranking lines can achieve the highest risk drop of 0.2548 MW, whereas the upgrading of the middle-ranking lines have very few effects. Particularly, the risk drops of the group of lowest ranking lines are negative. As seen from the corresponding Δr^+ and Δr^- of the lowest ranking lines, the probability decreases of their hidden failures can raise the failure probabilities of other critical lines and increase the system risk.

In addition, the risk variations in the three groups, which are 0.2548 MW, 0.0066 MW and 0.0310 MW respectively, are all smaller than the fluctuations of MC sampling method shown in Fig. 8. Therefore, the impacts of hidden failure probability changes on risks can be more accurately quantified by the proposed SF-network than the MC sampling method does.

Moreover, we test the method in different situations, where the loads are set to be as 100%, 130%, 150%, 200% and 250% of their original values respectively to cover situations from the best to the worst. Then, the rankings of the lines with hCCIs in the situations obtained by the method are listed in Table IV, where some of the identified most critical lines are highlighted in bolded fonts. The most critical lines can be identified in best and worst situations, despite the changes of the rankings due to different load flow levels.

TABLE IV
RANKINGS OF LINES WITH HCCIS IN DIFFERENT SITUATIONS

Ranking	100%		130%		150%		200%		250%	
	Line	hCCI	Line	hCCI	Line	hCCI	Line	hCCI	Line	hCCI
1	**3**	0.023	**4**	0.316	**4**	0.355	**10**	0.549	**4**	2.091
2	**4**	0.016	**3**	0.261	**5**	0.267	**4**	0.530	**7**	1.400
3	**10**	0.014	**5**	0.231	**3**	0.161	**5**	0.453	**5**	1.131
4	**7**	0.009	**10**	0.203	8	0.130	**3**	0.434	9	1.047
5	16	0.008	8	0.187	9	0.114	9	0.308	11	0.938
6	**5**	0.001	**7**	0.174	**10**	0.110	**7**	0.284	**10**	0.903
7	11	0.001	14	0.159	11	0.100	11	0.246	12	0.896
8	13	0.001	9	0.158	**7**	0.092	14	0.240	6	0.853
9	9	0	16	0.105	6	0.075	15	0.167	15	0.832
10	2	0	17	0.088	15	0.064	12	0.131	**3**	0.784
⋮	⋮		⋮		⋮		⋮		⋮	

B. Case 2: IEEE 118-bus System

The operation point is set as that of the IEEE 14-bus system in the last case. The failures of lines 96 and 66 are selected as the initial contingencies.

It takes 50260 searches to form the SF-network. Figure 11 shows the risk estimated by the SF-network method and the MC sampling method, where the converged risk is 206.49 MW.

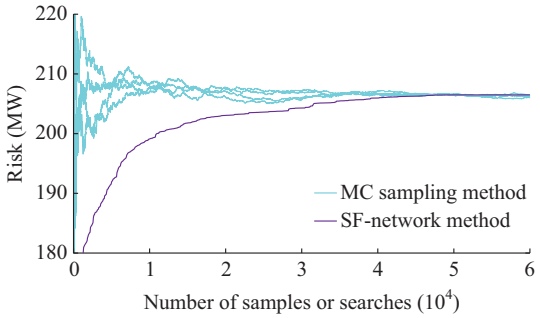

Fig. 11. Cascading failure risks estimated by MC sampling and SF-network methods by searching in IEEE 118-bus system.

Compared with the IEEE 14-bus system, forming the SF-network in this case demands longer time and more computations. It takes about 4642.09 s, whereas the MC sampling method needs about 7622.80 s to gather 50260 samples. As the sufficiency of searched hidden failures is preferred in this paper, the cumulated searched new hidden failures of both SF-network method and MC sampling method are shown in Fig. 12. Although both methods uncover new hid-

den failures, the MC sampling method can only trigger very limited hidden failures, which are about 4.7% of those searched by the SF-network method. Therefore, the SF-network method outperforms the MC sampling method in detecting hidden failures.

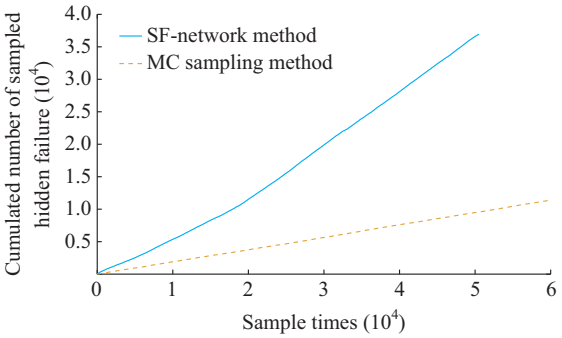

Fig. 12. New hidden failures searched by SF-network and MC sampling methods in IEEE 118-bus system.

The hCCIs of the lines in the IEEE 118-bus system are obtained by the SF-network and listed in Table V. Some lines are with zero hCCIs because they do not fail as hidden failures or their hidden failures are not critical at the states.

TABLE V
HCCIS OF LINES IN IEEE 118-BUS SYSTEM

Ranking	Line	hCCI	Ranking	Line	hCCI
1	115	0.9274000	31	113	0.0000174
2	117	0.5917000	⋮	⋮	⋮
3	65	0.0598000	163	66	0
4	60	0.0241000	164	75	0
⋮	⋮	⋮	165	95	0
28	12	0.0000526	166	51	0
29	112	0.0000494	⋮	⋮	⋮
30	136	0.0000350			

To verify the identified critical hidden failure lines, three groups of lines (the top-ranking lines 115, 117, 65, 60, the middle-ranking lines 12, 112, 136, 113 and the low-ranking lines 66, 75, 95, 51) are chosen based on their rankings in the table. The hidden failure probabilities of the chosen lines are reduced from 0.01 to 0.001 to simulation system improvement measures. Re-estimating the risks by the calculations in the SF-network takes about 17 s, which is dramatically shorter than the time consumptions of forming the SF-network or MC sampling methods. Table VI shows that upgrading the most critical hidden failure lines can result in the largest risk drop.

The CCDFs of the blackouts after upgrading different groups of lines are given in Fig. 13. It can be observed that the hidden failures mainly influence the occurrence probabilities of larger blackouts. We take the blackouts with losses larger than 1200 MW as the severe blackouts. The occurrence numbers of the severe blackouts are 18, 17, 13 and 5 in the original, low-ranking, middle-ranking and top-ranking scenarios, respectively.

TABLE VI
RISK VARIATION DUE TO HIDDEN FAILURE PROBABILITY CHANGES OF IEEE 118-BUS SYSTEM

Line group	Lines	Δr	Δr^+	Δr^-
Top ranking	115, 117, 65, 60	1.0036	2.0405	−1.0369
Middle ranking	12, 112, 136, 113	−0.0125	0.0233	−0.0358
Low ranking	66, 75, 95, 51	−0.0261	0.0263	−0.0524

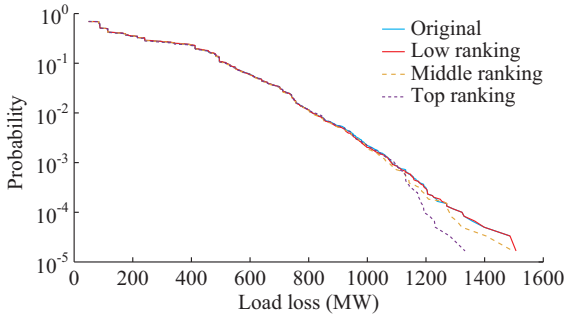

Fig. 13. CCDFs of blackouts after upgrading different groups of lines in IEEE 118-bus system.

According to [34], the minimum number to conclude that the probabilities of the severe blackouts in the other scenarios are higher than those in the top-ranking scenario with a confidence level of 95% is 11. Therefore, the occurrence probability of the severe blackouts in the top-ranking scenario is the lowest among the four scenarios with a confidence level of 95%.

V. CONCLUSION

This paper proposes a SF-network method to identify the critical hidden failure lines. The searching to form the SF-network insures that sufficient hidden failures are searched and the duplicated searches of failure chains are avoided. When the SF-network is formed, the state and failure value calculations in the SF-network can efficiently obtain the indices to identify the critical hidden failure lines and achieve risk estimations for verifications of the identification. In comparison with the commonly used sampling based methods, the proposed method can achieve not only more accurate risk estimations, but also high efficiency in risk re-estimations. The simulations validate that the accuracy and efficiency of the proposed method.

Our future work includes forming the SF-network by less searches and applications of the method in more complicated analyses.

REFERENCES

[1] M. Vaiman, K. Bell, Y. Chen *et al.*, "Risk assessment of cascading outages: methodologies and challenges," *IEEE Transactions on Power Systems*, vol. 27, no. 2, pp. 631-641, May 2012.
[2] O. P. Veloza and F. Santamaria, "Analysis of major blackouts from 2003 to 2015: classification of incidents and review of main causes," *The Electricity Journal*, vol. 29, no. 7, pp. 42-49, Sept. 2016.
[3] J. Thorp, A. Phadke, S. Horowitz *et al.*, "Anatomy of power system disturbances: importance sampling," *International Journal of Electrical Power & Energy Systems*, vol. 20, no. 2, pp. 147-152, Feb. 1998.
[4] A. Phadke and J. S. Thorp, "Expose hidden failures to prevent cascad-

ing outages in power systems," *IEEE Computer Applications in Power*, vol. 9, no. 3, pp. 20-23, Jul. 1996.
[5] J. Chen, J. S. Thorp, and I. Dobson, "Cascading dynamics and mitigation assessment in power system disturbances via a hidden failure model," *International Journal of Electrical Power & Energy Systems*, vol. 27, no. 4, pp. 318-326, May 2005.
[6] L. Zhao, X. Li, M. Ni *et al.*, "Review and prospect of hidden failure: protection system and security and stability control system," *Journal of Modern Power Systems and Clean Energy*, vol. 7, no. 6, pp. 1735-1743, Nov. 2019.
[7] A. G. Phadke, P. Wall, L. Ding *et al.*, "Improving the performance of power system protection using wide area monitoring systems," *Journal of Modern Power Systems & Clean Energy*, vol. 4, no. 3, pp. 319-331, Jul. 2016.
[8] Z. Jiao, H. Gong, and Y. Wang, "A d-s evidence theory-based relay protection system hidden failures detection method in smart grid," *IEEE Transactions on Smart Grid*, vol. 9, no. 3, pp. 2118-2126, Sept. 2016.
[9] H. F. Albinali and A. P. S. Meliopoulos, "Resilient protection system through centralized substation protection," *IEEE Transactions on Power Delivery*, vol. 33, no. 3, pp. 1418-1427, Jun. 2018.
[10] Y. Cai, Y. Cao, Y. Li *et al.*, "Cascading failure analysis considering interaction between power grids and communication networks," *IEEE Transactions on Smart Grid*, vol. 7, no. 1, pp. 530-538, Jan. 2016.
[11] Y. Han, C. Guo, S. Ma *et al.*, "Modeling cascading failures and mitigation strategies in pmu based cyber-physical power systems," *Journal of Modern Power Systems & Clean Energy*, vol. 6, no. 5, pp. 944-957, Sept. 2018.
[12] Y. Wang and H. Pham, "A multi-objective optimization of imperfect preventive maintenance policy for dependent competing risk systems with hidden failure," *IEEE Transactions on Reliability*, vol. 60, no. 4, pp. 770-781, Dec. 2011.
[13] B. Liu, R. Yeh, M. Xie *et al.*, "Maintenance scheduling for multicomponent systems with hidden failures," *IEEE Transactions on Reliability*, vol. 66, no. 4, pp. 1280-1292, Dec. 2017.
[14] K. Bae and J. S. Thorp, "A stochastic study of hidden failures in power system protection," *Decision Support Systems*, vol. 24, no. 3, pp. 259-268, Jan. 1999.
[15] D. C. Elizondo, J. L. Ree, A. G. Phadke *et al.*, "Hidden failures in protection systems and their impact on wide-area disturbances," in *Proceedings of 2001 IEEE PES Winter Meeting*, Columbus, USA, Jan. 2001, pp. 710-714.
[16] F. Yang, A. S. Meliopoulos, G. J. Cokkinides *et al.*, "Effects of protection system hidden failures on bulk power system reliability," in *Proceedings of 38th North American Power Symposium*, Carbondale, USA, Sept. 2006, pp. 517-523.
[17] N. A. Salim, M. M. Othman, I. Musirin *et al.*, "Risk assessment of cascading collapse considering the effect of hidden failure," in *Proceedings of 2012 IEEE International Conference on Power and Energy (PECon)*, Kota, Malaysia, Dec. 2012, pp. 778-783.
[18] S. Mei, F. He, X. Zhang *et al.*, "An improved opa model and blackout risk assessment," *IEEE Transactions on Power Systems*, vol. 24, no. 2, pp. 814-823, Apr. 2009.
[19] O. A. Mousavi, R. Cherkaoui, and M. Bozorg, "Blackouts risk evaluation by Monte-Carlo simulation regarding cascading outages and system frequency deviation," *Electric Power Systems Research*, vol. 89, pp. 157-164, Aug. 2012.
[20] Y. Cai, Y. Li, Y. Cao *et al.*, "Modeling and impact analysis of interdependent characteristics on cascading failures in smart grids," *International Journal of Electrical Power & Energy Systems*, vol. 89, pp. 106-114, Jul. 2017.
[21] Z. Ma, C. Shen, F. Liu *et al.*, "Fast screening of vulnerable transmission lines in power grids: a pagerank-based approach," *IEEE Transactions on Smart Grid*, vol. 10, no. 2, pp. 1982-1991, Dec. 2017.
[22] J. Guo, F. Liu, J. Wang *et al.*, "Toward efficient cascading outage simulation and probability analysis in power systems," *IEEE Transactions on Power Systems*, vol. 33, no. 3, pp. 2370-2382, May 2018.
[23] S. Tamronglak, S. Horowitz, A. Phadke *et al.*, "Anatomy of power system blackouts: preventive relaying strategies," *IEEE Transactions on Power Delivery*, vol. 11, no. 2, pp. 708-715, Apr. 1996.
[24] L. Li, H. Wu, Y. Song *et al.*, "A state-failure-network method to identify critical components in power systems," *Electric Power Systems Research*, vol. 181, Apr. 2020.
[25] L. Li, H. Wu, and Y. Song, "Temporal difference learning based critical component identifying method with cascading failure data in power systems," in *Proceedings of 2018 IEEE PES General Meeting (PESGM)*, Portland, USA, Aug. 2018, pp. 1-5.
[26] R. Yao, S. Huang, K. Sun *et al.*, "A multi-timescale quasi-dynamic model for simulation of cascading outages," *IEEE Transactions on Power Systems*, vol. 31, no. 4, pp. 3189-3201, Sept. 2015.
[27] A. Lipowski and D. Lipowska, "Roulette-wheel selection via stochastic acceptance," *Physica A: Statistical Mechanics and its Applications*, vol. 391, no. 6, pp. 2193-2196, Mar. 2012.
[28] Y. Jia, Z. Xu, L. Lai *et al.*, "Risk-based power system security analysis considering cascading outages," *IEEE Transactions on Industrial Informatics*, vol. 12, no. 2, pp. 872-882, Apr. 2016.
[29] B. A. Carreras, V. E. Lynch, M. Sachtjen *et al.*, "Modeling blackout dynamics in power transmission networks with simple structure," in *Proceedings of the 34th Annual Hawaii International Conference on System Sciences*, Washington DC, USA, Jan. 2001, pp. 719-727.
[30] S. Soltan, D. Mazauric, and G. Zussman, "Analysis of failures in power grids," *IEEE Transactions on Control of Network Systems*, vol. 4, no. 2, pp. 288-300, Nov. 2015.
[31] R. Yao, S. Huang, K. Sun *et al.*, "Risk assessment of multi-timescale cascading outages based on markovian tree search," *IEEE Transactions on Power Systems*, vol. 32, no. 4, pp. 2887-2900, Oct. 2016.
[32] Power Systems Engineering Research Center (PSERC). (2019, Jun.). Matpower (version 7.0). [Online]. Available: https://matpower.org/
[33] L. Che, X. Liu, Y. Wen *et al.*, "A mixed integer programming model for evaluating the hidden probabilities of *N–k* line contingencies in smart grids," *IEEE Transactions on Smart Grid*, vol. 10, no. 1, pp. 1036-1045, Oct. 2017.
[34] I. Dobson, B. A. Carreras, and D. E. Newman, "How many occurrences of rare blackout events are needed to estimate event probability?" *IEEE Transactions on Power Systems*, vol. 28, no. 3, pp. 3509-3510, Aug. 2013.

Linzhi Li received the B.E. degree in electrical engineering from Zhejiang University, Hangzhou, China, in 2014. He is currently pursuing the Ph.D. degree in electrical engineering in Zhejiang University. His research interests include the simulation of cascading failures, risk assessment and management.

Lu Liu received the bachelor's degree in electrical engineering at Zhejiang University, Hangzhou, China, in 2018. She is currently pursuing the M.S. degree in the same department. Her research interests include power system cascading failure analysis and stability study.

Hao Wu received the bachelor's degree from Shanghai Jiao Tong University, Shanghai, China, in 1996, and the master's and Ph.D. degrees from Zhejiang University, Hong Kong, China, Hangzhou, China, in 1999 and 2003, respectively, all in electrical engineering. He joined Zhejiang University in 2002, and visited Hong Kong Polytechnic University, Hong Kong, China, in 2003-2004 and University of Wisconsin Madison in 2009-2011. His current research interests include power system operation and stability, uncertainty analysis, cascading failure, load characteristic, and load modeling.

Yonghua Song received the B.E. degree from the Chengdu University of Science and Technology, Chengdu, China, in 1984, and the Ph.D. degree from China Electric Power Research Institute, Beijing, China, in 1989, both in electrical engineering. Currently, he is Rector of the University of Macau, Macau, China, and also an Adjunct Professor at the College of Electrical Engineering, Zhejiang University, Hangzhou, China. He was Executive Vice President of Zhejiang University from 2012 to 2017. He was elected Vice President of the Chinese Society for Electrical Engineering (CSEE) and appointed Chairman of the International Affairs Committee of the CSEE in 2009. In 2004, he was elected as a Fellow of the Royal Academy of Engineering, U.K. His current research interests include smart grid, electricity economics, and operation and control of power systems.

Dunwen Song is currently a Senior Engineer in China Electric Power Research Institute, Beijing, China. His research interests include power system stability analysis and control, and power system simulation tool development.

Yi Liu is currently a Senior Engineer in State Grid Henan Electric Power Company, Zhengzhou, China. His research interests include power system operation analysis and dispatching.